

Many-body renormalization of Landau levels in graphene due to screened Coulomb interaction

Alexey A. Sokolik^{1,2} and Yurii E. Lozovik^{1,2,3,*}

¹*Institute for Spectroscopy, Russian Academy of Sciences, 142190 Troitsk, Moscow, Russia*

²*National Research University Higher School of Economics, 109028 Moscow, Russia*

³*Dukhov Research Institute of Automatics (VNIIA), 127055 Moscow, Russia*

Renormalization of Landau level energies in graphene in strong magnetic field due to Coulomb interaction is studied theoretically, and calculations are compared with two experiments on carrier-density dependent scanning tunneling spectroscopy. An approximate preservation of the square-root dependence of the energies of Landau levels on their numbers and magnetic field in the presence of the interaction is examined. Many-body calculations of the renormalized Fermi velocity with the statically screened interaction taken in the random-phase approximation show good agreement with both experiments. The crucial role of the screening in achieving quantitative agreement is found. The main contribution to the observed rapid logarithmic growth of the renormalized Fermi velocity on approach to the charge neutrality point turned out to be caused not by mere exchange interaction effects, but by weakening of the screening at decreasing carrier density. The importance of a self-consistent treatment of the screening is also demonstrated.

I. INTRODUCTION

Many-body effects of Coulomb interaction between massless Dirac electrons in graphene are widely studied both theoretically and in a series of transport and optical experiments [1–3]. Renormalization of the electron Fermi velocity to higher values, showing logarithmic divergence upon approaching the charge neutrality point [3, 4], is the most prominent signature.

Graphene in quantizing magnetic field serves as a perspective system where both quantum single-particle and many-body effects can be studied [5–8]. According to an idealized single-particle picture, electrons in monolayer graphene in the magnetic field B occupy the relativistic Landau levels

$$E_n = \text{sgn}(n) v_F \sqrt{2|n|B\hbar/c}, \quad n = 0, \pm 1, \pm 2, \dots, \quad (1)$$

where $v_F \approx 10^6$ m/s is the Fermi velocity. In the presence of Coulomb interaction, many-body effects cause renormalization of these energies to new values E_n^* . Thus the problem of systematization and theoretical description of the interaction induced energy shifts $E_n^* - E_n$ arises.

In several experiments [9–16] on scanning tunneling spectroscopy of graphene in magnetic field, E_n^* were measured and turned out to be in agreement with the same square-root law $E_n^* \propto \text{sgn}(n) \sqrt{|n|B}$ as for noninteracting electrons. This admits an effective single-particle description of the energy levels in a many-body system using the phenomenological renormalized Fermi velocity v_F^* :

$$E_n^* = \text{sgn}(n) v_F^* \sqrt{2|n|B\hbar/c}. \quad (2)$$

However some of these experiments [15, 16], where the carrier density in graphene n_e was varied, reported the

growth of v_F^* when the density of electrons or holes decreases approaching the charge neutrality point $n_e = 0$. This effect cannot be described by an effective single-particle picture with a fixed v_F^* . It has intrinsically many-body character and bears similarities to renormalization of the effective Fermi velocity predicted and observed in the absence of magnetic field [3, 4].

Deviations of observable energies of inter-Landau level transitions from single-particle theory predictions, discovered in cyclotron resonance [17–20] and magneto-Raman scattering [21–24] experiments, are another manifestation of many-body effects in graphene in magnetic field. Proper theoretical description of these deviations requires taking into account not only renormalization of individual Landau levels, but also the excitonic effects of electron-hole interaction in a final state [22, 24–32]. The splitting of Landau levels in very strong magnetic field can be also mentioned as a striking signature of many-body effects (see, e.g., [5, 7] and references therein).

In this paper, we focus our theoretical study on renormalization of Landau levels in monolayer graphene, which was observed in the scanning tunneling spectroscopy experiments [15, 16] where the variations of v_F^* versus n_e were measured. Our calculations are based on evaluating the mean-field exchange energies of electrons at Landau levels using the statically screened Coulomb interaction, as described in Sec. II.

Then in Sec. III we analyze the behavior of the renormalized energies and discuss the validity of approximating a set of E_n^* with the single formula (2), which is routinely applied in the experimental works [9–16].

In Sec. IV we fit the experimental data with our calculations in different approximations, both with and without screening. The bare Fermi velocity $v_F = 0.85 \times 10^6$ m/s and the realistic dielectric constants allow us to achieve good agreement with the experiments. We show that the main cause of the renormalized Fermi velocity growth at decreasing carrier density is not the Landau-level filling factor dependence of electron exchange ener-

*Electronic address: lozovik@isan.troitsk.ru

gies, but the weakening of the screening. Therefore taking into account the interaction screening is crucial for appropriate description of the many-body effects. The important role of the self-consistent weakening of the screening is also demonstrated. Our conclusions are presented in Sec. V.

II. THEORETICAL MODEL

The conventional approach [25–37] to treat the interaction-induced renormalization of Landau level energies is based on the Hartree-Fock approximation, where the renormalized energy

$$E_n^* = E_n + \Sigma_n - \Sigma_0 \quad (3)$$

consists of the bare single-particle energy E_n and of the exchange self-energy Σ_n . To maintain the Dirac point location at $E = 0$, the renormalized energy $E_0^* = \Sigma_0$ of the zeroth Landau level was subtracted. The self-energy

$$\Sigma_n = - \sum_{n'k'} f_{n'} \langle \psi_{nk}, \psi_{n'k'} | V | \psi_{nk}, \psi_{n'k'} \rangle \quad (4)$$

is a result of virtual processes of exchanging an electron on the n th level with other electrons in all occupied n' th levels; $f_{n'}$ are the occupation numbers of these levels ($0 \leq f_{n'} \leq 1$), and $\langle \psi_{nk}, \psi_{n'k'} | V | \psi_{nk}, \psi_{n'k'} \rangle$ are the exchange matrix elements of the Coulomb interaction $V(\mathbf{r})$. The single-particle states ψ_{nk} are characterized by the Landau level number n and by an additional quantum number k , which accounts for a Landau level degeneracy.

To handle the logarithmic divergence of the self-energies (4) upon summation over the negative-energy Landau levels n' , the physically motivated cutoff $n' \geq -n_c$ should be introduced [25–30]. Because of its degeneracy, each Landau level hosts $geB/2\pi\hbar c$ electrons per unit area, where $g = 4$ is the fourfold spin and valley degeneracy factor. Assuming that n_c occupied Landau levels below the Dirac point in charge neutral graphene should host two electrons per elementary cell of the area $S_0 = a^2\sqrt{3}/2$ ($a \approx 2.46 \text{ \AA}$), we get

$$n_c = \frac{8\pi\hbar c}{\sqrt{3}ga^2eB} \approx \frac{39600}{B [\text{T}]} \quad (5)$$

As noted in [36], a numerical calculation and summation of large numbers, typically tens of thousands, of matrix elements in (4) presents a separate computational problem. The formula (5) contains some uncertainties due to inaccuracy of the Dirac low-energy model away from the Dirac point, but our estimates show their influence of the calculation results is weak: for example, changing the number 39600 in the numerator of (5) by 20% results in the change of the calculated E_n^* by about 1%.

In the most of theoretical works [25–31, 33, 37], the unscreened Coulomb interaction $v(r) = e^2/\epsilon r$ was used to calculate the exchange energies (4). Here ϵ is the dielectric constant of a surrounding medium, which varies

from $\epsilon = 1$ for suspended graphene to $\epsilon \sim 10 - 20$ for graphene on a graphite substrate [22, 32]. In our earlier paper [32] we showed that the screening of Coulomb interaction by a polarizable gas of massless electrons of graphene should be taken into account to achieve quantitative agreement with the experiments on cyclotron resonance and magneto-Raman scattering [17, 18, 21, 22]. In this work we follow the similar approach and use the statically screened interaction when calculate the matrix elements in (4). Its Fourier transform is

$$V(q) = \frac{v(q)}{1 - v(q)\Pi(q, 0)}, \quad (6)$$

where $v(q) = 2\pi e^2/\epsilon q$ is the Fourier transform of the unscreened interaction $v(r)$, $\Pi(q, \omega)$ is the irreducible polarizability of graphene in magnetic field. In the random-phase approximation, the latter is calculated by taking into account all virtual electron transitions between filled and empty Landau levels,

$$\Pi(q, 0) = g \sum_{nn'} F_{nn'}(q) \frac{f_n - f_{n'}}{E_n - E_{n'}}, \quad (7)$$

where $F_{nn'}(q)$ are the Landau level form factors (see the details in [5, 38–42]). Note that the statically screened interaction was also used in [34–36] to analyze possible spontaneous symmetry breaking and gap generation scenarios. Generally, full dynamical treatment of the screening can provide more accurate results than in the static approximation, although the computational procedure in this case becomes very demanding.

Let us examine how the screened interaction $V(q)$ depends on the parameters v_F , ϵ of the model. Via the energy denominators, the polarizability (7) scales with the Fermi velocity as $\Pi(q, 0) \propto v_F^{-1}$, thus the quantity $v(q)\Pi(q, 0)$ in the denominator of (6) scales as

$$v(q)\Pi(q, 0) \propto r_s \equiv \frac{e^2}{\epsilon\hbar v_F}. \quad (8)$$

The dimensionless parameter r_s (sometimes referred to as the graphene analogue α of the fine structure constant [3, 5]) is conventionally used to characterize the relative strength of Coulomb interaction. However in our approach it actually measures the strength of the screening due to the linear scaling between r_s and $\Pi(q, 0)$ in (6).

Another important point is a necessity of a self-consistent treatment of the screening, i.e. calculation of the polarizability using the electron Green functions, which are already “dressed” by many-body interaction effects. In the simplest approach, this reduces to a calculation of the energy differences in the denominators of (7) with the renormalized energies E_n^* instead of the bare ones E_n . Since the typical renormalized Fermi velocities v_F^* can be up to 60% higher than the bare velocity v_F [32] (and the same is true for the energy differences), the self consistent screening can be appreciably weaker than in the random-phase approximation. Full self-consistent

treatment of the screening is highly computationally demanding so we use the simplified model where $\Pi(q, 0)$ retains its functional form but becomes proportionally reduced by the factor $v_F/v_F^* < 1$. This is achieved by replacing v_F in the definition of r_s by v_F^* , so the resulting r_s , which appears in the denominator of (6), becomes smaller than in the case of the non self-consistent screening. The value of v_F^* in the prefactor of $\Pi(q, 0)$ can be taken either from experiments or from theoretical calculations.

The assumption of the unchanged functional form of $\Pi(q, 0)$ is reasonable because the renormalized Landau level energies retain their dependence $E_n^* \propto \text{sgn}(n)\sqrt{|n|B}$ on n, B with sufficiently high accuracy (as confirmed in the next section) and only change by the overall numerical factor v_F^*/v_F . The remote levels with $|n| \gg 1$ can deviate from this regularity because of a breakdown of the Dirac model at high energies, but their contribution to $\Pi(q, 0)$ is not critical due to small form factors $F_{nn'}(q)$ and large energy denominators.

In order to analyze the role of the screening, we carry out the calculations using, similarly to [32], the following four screening models:

- (1) unscreened Coulomb interaction, when $r_s = 0$;
- (2) screened interaction, $r_s = e^2/\varepsilon\hbar v_F$;
- (3) self-consistently screened interaction with $r_s = e^2/\varepsilon\hbar\langle v_F^* \rangle$, where $\langle v_F^* \rangle$ is the average value of the experimental renormalized Fermi velocity in the measured range of carrier densities;
- (4) self-consistently screened interaction with a variable screening strength $r_s = e^2/\varepsilon\hbar v_F^*(n_e)$ where r_s and $v_F^*(n_e)$ are calculated at each n_e iteratively: initially $v_F^* = v_F$ and then in each iteration the next value of v_F^* is extracted from a set of E_n^* calculated with $r_s = e^2/\varepsilon\hbar v_F^*$ determined by the previous value of v_F^* (typically 5 iterations are sufficient to achieve convergence).

The 3rd and 4th models consider the screening to be self-consistently weakened with respect to that in the random-phase approximation: in the 3rd model the magnitude of this weakening is estimated on the basis of experimental data, while in the 4th model it is calculated theoretically. We will show below that the 3rd and 4th models provide much better agreement with the experimental data indicating the importance of the self-consistent treatment of the screening.

III. EVALUATION OF v_F^*

The renormalized Landau level energies (3) depend on the Landau level number n , magnetic field B and, importantly, on the filling factor ν . The latter equals to 0 in undoped graphene, when the zeroth level is half-filled, while a complete filling of each new Landau level increases ν by 4 because of the fourfold spin-valley degeneracy of electron states in graphene [5]. The filling

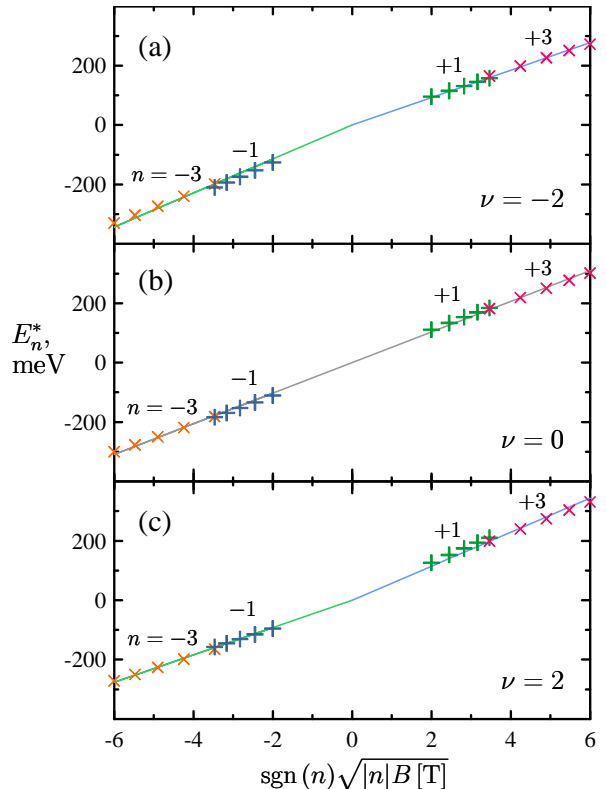


FIG. 1: Renormalized Landau level energies E_n^* as functions of $\text{sgn}(n)\sqrt{|n|B}$ calculated with $v_F = 0.85 \times 10^6$ m/s, $\varepsilon = 2$, $r_s = 0.87$ at different filling factors ν . Each level with the number $n = -3, -1, +1, \text{ or } +3$ is presented by the series of five points (crosses) at magnetic fields $B = 4, 6, 8, 10, 12$ T. The linear fits for these sets of points on the electron and hole sides are shown by the solid lines.

factor is related to the carrier density as

$$n_e = \frac{eB}{2\pi\hbar c} \nu \approx 0.0242 \nu \times 10^{12} \text{ cm}^{-2} \times B [\text{T}] \quad (9)$$

and reaches the values up to $\nu \approx \pm(15 - 30)$ in the experiments [15, 16].

It was commonly accepted [9–16] that $E_n^* \propto \text{sgn}(n)\sqrt{|n|B}$ at fixed n_e and varying (n, B) . However the recent experiments [21–23] on magneto-Raman scattering revealed the visible dependence of v_F^* on a magnetic field of the form $v_F^* \approx C_1 - C_2 \ln B$. Its origin can be traced theoretically from Eq. (4): as the sum has a logarithmic divergence which have been regularized using the cutoff (5), so the result will be logarithmically dependent on a cutoff position and hence on B .

In Fig. 1, the typical dependence of E_n^* on n, B , and ν is investigated. The calculations are carried out under the typical conditions of the experiment [15] in the 3rd aforementioned screening model (see Sec. III). Analyzing behavior of the linear fits (2) as well as deviations of individual points from these fits, we can note the following regularities:

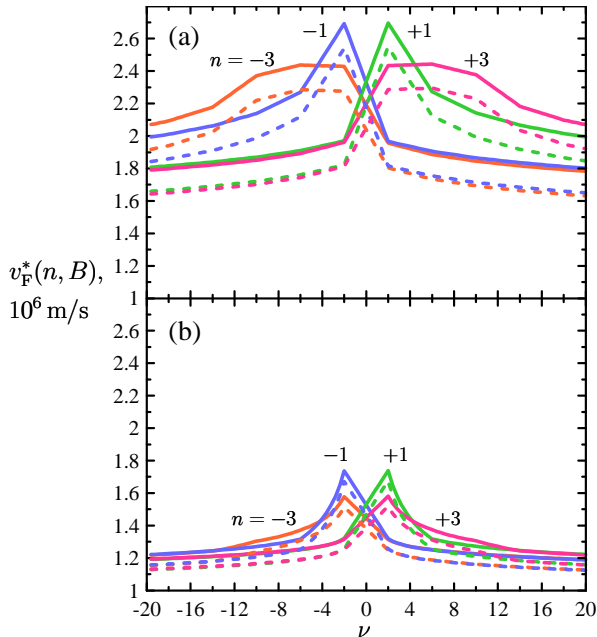


FIG. 2: Effective Fermi velocities $v_F^*(n, B)$ [see Eq. (10)] as functions of the filling factor ν , calculated at $v_F = 0.85 \times 10^6$ m/s, $\epsilon = 2$ (a) with the unscreened interaction, and (b) with the self-consistently screened interaction ($r_s = 0.87$). Solid and dashed lines correspond, respectively, to magnetic fields $B = 4$ and 12 T.

(a) The effective Fermi velocities

$$v_F^*(n, B) = \frac{E_n^*}{\text{sgn}(n)\sqrt{2|n|B\hbar/c}} \quad (10)$$

assigned to individual points (n, B) always decrease at increasing B . For example, the $n = +3$ points in Fig. 1(a) lie slightly above the linear fit at low B and slightly below the fit at high B . This conforms both the experiments and the theory demonstrating the logarithmic decrease of v_F^* versus B [21–23, 29–32].

(b) The electron-hole asymmetry between Fig. 1(a) and Fig. 1(c) implies that $v_F^*(n, B)$ is higher when n and ν have the same sign (both are on the electron or on the hole side) and lower when they have different signs (one is on the electron, and the other is on the hole side). In other words, the energies of those Landau levels which lie closer to the Fermi level undergo stronger renormalization to higher values.

(c) The effect of the upward renormalization of the Fermi velocity is generally more pronounced for Landau levels with smaller $|n|$. For example, in Fig. 1 it is appreciably stronger for $n = \pm 1$ than for $n = \pm 3$.

The same regularities are presented more clearly in Fig. 2, where the effective Fermi velocities $v_F^*(n, B)$ are plotted as functions of the filling factor ν . Without the screening [Fig. 2(a)], $v_F^*(n, B)$ are the piecewise-linear functions of ν with the kinks at $\nu = \pm 2, \pm 6, \pm 10, \dots$, where an integer number of Landau levels is filled. This

behavior is dictated by Eq. (4), which implies a linear change of E_n^* versus $f_{n'}$ during filling of each Landau level. The screening [Fig. 2(b)] significantly reduces the effective Fermi velocities and removes the strict piecewise-linear behavior because now the screened interaction $V(q)$ also changes during the filling of each Landau level. Nevertheless, an approximate piecewise linearity survives. Note that the evident piecewise linear dependence was observed in the recent magneto-Raman scattering experiment [24].

In the scanning tunneling spectroscopy experiments [9–16], the values of v_F^* were evaluated by approximating some set of measured E_n^* with different (n, B) by the formula (2). In [15, 16], this procedure was repeated at each density n_e do obtain the $v_F^*(n_e)$ relationship. The presented analysis allows us to conclude that the result of such evaluation can depend on a taken set of (n, B) . Generally, higher B and $|n|$ lead to lower v_F , and the electron-hole asymmetry can influence the result, though in the most cases the approximation (2) is quite accurate.

IV. COMPARISON WITH EXPERIMENTS

In the first considered experiment [15], graphene on a SiO_2 substrate was studied and the fitting of the energies of several lowest Landau levels $n = -3, -2, -1, 0$ at magnetic fields in the range $B = 4 - 8$ T was reported. The carrier densities n_e were taken at rather low hole doping levels not exceeding $-3 \times 10^{12} \text{ cm}^{-2}$. As shown in the inset in Fig. 3, v_F^* in spite of some scattering of the experimental points demonstrates the clear growing trend at decreasing $|n_e|$ which can be approximated by the logarithmic function

$$\frac{v_F^*(n_e)}{10^6 \text{ m/s}} = \left(1.363 - 0.192 \ln \frac{|n_e|}{10^{12} \text{ cm}^{-2}} \right). \quad (11)$$

To reproduce these results theoretically, we have taken the set of 20 energies E_n^* with $n = -3, -2, -1, 0$ at $B = 4, 5, 6, 7, 8$ T and evaluated v_F^* at each n_e by their least-square fitting with the formula (2). Note that even at fixed n_e the filling factor ν varies in the calculations when B is changed due to Eq. (5).

Each of the four calculation models, described in Sec. II, need the bare Fermi velocity v_F and the dielectric constant of surroundings ϵ as the parameters. As known (see, e.g., [32, 43]), the phenomenological values of v_F used by different authors to describe such many-body renormalized observables of graphene as electron transition energies or quantum capacitance fall in the range $(0.8 - 1) \times 10^6$ m/s.

Table I shows the results of adjusting ϵ at several selected values of v_F in the four models, made in order to achieve the best least-square fits of the experimental points $v_F^*(n_e)$. In the absence of the screening, we have obtained the overestimated values of ϵ because higher external dielectric constants are required to simulate the screening of the interaction caused by both surrounding

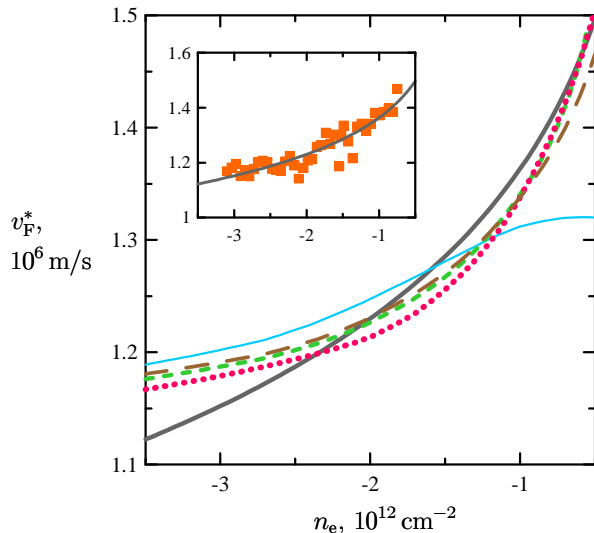


FIG. 3: The best fits to the experimental [15] dependence of v_F^* on the carrier density n_e at $v_F = 0.85 \times 10^6$ m/s: with the unscreened interaction (thin solid line), screened interaction (short-dashed line), self-consistently screened interaction with the constant r_s (long-dashed line) and self-consistently screened interaction with the iteratively calculated varying r_s (dotted line). The logarithmic trend (11) of the experimental Fermi velocity growth is shown by thick solid line. Inset shows the experimental points (squares) and the extracted logarithmic trend.

medium and graphene electrons. On the contrary, the non-self-consistent static screening requires very low ϵ (sometimes even unphysically smaller than 1), which indicates an overestimation of the actual screening in this model. Finally, the two self-consistent screening models provide more realistic values of ϵ . To determine r_s in the 3rd model, we take the experimental average $\langle v_F^* \rangle = 1.253 \times 10^6$ m/s.

Similarly to our earlier work [32] and to [44], we find the bare Fermi velocity $v_F = 0.85 \times 10^6$ m/s as providing the best agreement of the many-body theory with the experiments. In the most accurate 3rd and 4th screening models, we get $\epsilon \approx 2$ which is close to the experimental

TABLE I: Dielectric constants of surrounding medium ϵ , which provide the best least-square fittings of the experimental data from Ref. [15] at several selected v_F . The fittings are carried out in four screening models, described in Sec. II.

v_F , 10^6 m/s	Unscreened	Screened	Self-cons.	Self-cons.
	interaction $r_s = 0$	interaction $r_s = \frac{e^2}{\epsilon \hbar v_F}$	screening $r_s = \frac{e^2}{\epsilon \hbar \langle v_F^* \rangle}$	screening $r_s = \frac{e^2}{\epsilon \hbar v_F^*(n_e)}$
0.8	5.83	< 0.01	1.40	1.46
0.85	6.54	0.35	2.01	1.95
0.9	7.45	1.36	2.79	2.60
1	10.31	4.31	5.33	4.70

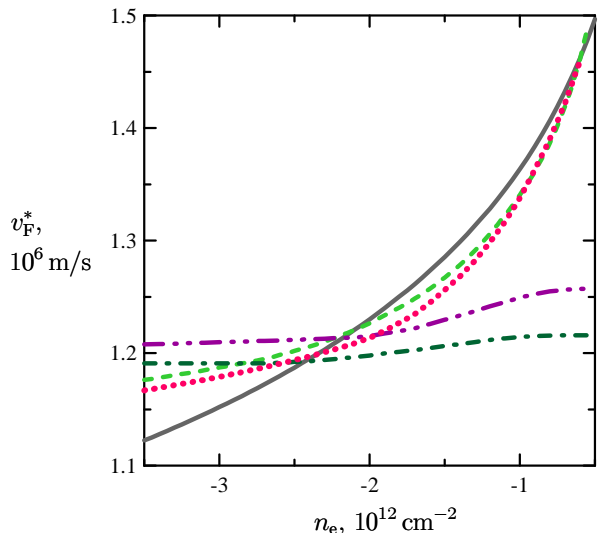


FIG. 4: The same as Fig. 3, but only the models of the screened interaction (short-dashed line) and the self-consistently screened interaction with the iteratively calculated varying r_s (dotted line) are retained. Calculations in the same approximations but with the screening corresponding to the constant filling factor $\nu = -14$ are shown by, respectively, dash-dotted and dash-double-dotted lines. The logarithmic trend (11) of the experimental Fermi velocity growth is shown by thick solid line.

effective dielectric constant 2.5 arising when graphene is supported by the SiO_2 substrate from the bottom.

Fig. 3 shows the best fits at this v_F in four screening models, which correspond to the entries in the second row of Table I. Due to noticeable scattering of the experimental points (see the inset), it is better to compare the calculations not with the points themselves, but with their smooth logarithmic trend (11). The 3rd and 4th self-consistent screening models, which use r_s determined from either experimental or from iteratively calculated v_F^* , are the best in reproducing the experimental trend in the whole range of n_e with realistic ϵ .

As seen, the unscreened interaction does not describe the rapid growth of v_F^* on approach to the charge neutrality point even at the optimal ϵ . Therefore the conventional first-order logarithmic renormalization of the Fermi velocity [4] fails to reproduce the experiment [15] with realistic model parameters v_F , ϵ . The screening resolves this problem because at smaller $|n_e|$ the polarizability of graphene decreases and thus the upward renormalization of the Fermi velocity becomes stronger. To illustrate this point, we compare in Fig. 4 the calculations in the 2nd and 4th screening models, which are carried out, on the one hand, with the screening correctly dependent on n_e , and, on the other hand, with a constant polarizability “frozen” at the typical filling factor $\nu = -14$. We see that the latter calculations, which take into account only changes of the occupation numbers $f_{n'}$ in (4) on varying the carrier density, does not

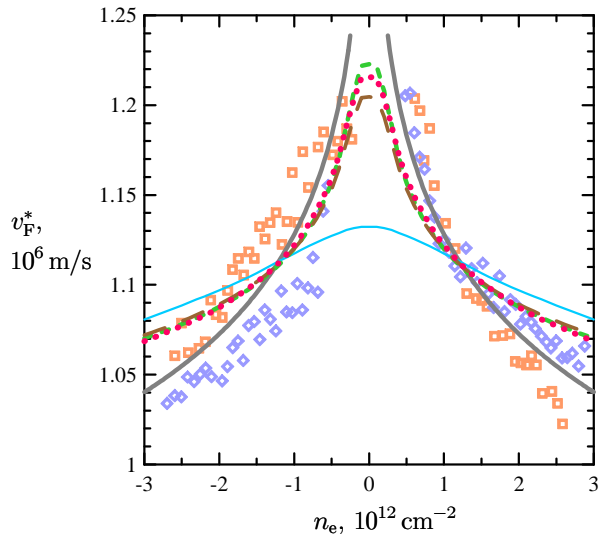


FIG. 5: The best fits to the experimental points [16] (squares and diamonds, corresponding to electron and hole puddles) on v_F^* versus carrier density n_e at $v_F = 0.85 \times 10^6$ m/s. The designations of the curves are the same as in Fig. 3. The logarithmic trend (12) of the experimental data is shown by thick solid line.

reproduce the rapid growth of v_F^* . So the dependence of $\Pi(q, 0)$ on n_e is crucial to achieve agreement with the experiment.

In the second considered experiment [16], graphene on a hexagonal boron nitride substrate was studied and energies of larger number of Landau levels, typically $n = -8, -7, \dots, +7, +8$, at magnetic fields $B = 2$ and 5 T were measured. Two sets of experimental points $v_F^*(n_e)$ were obtained in the range $-3 \times 10^{12} \text{ cm}^{-2} < n_e < 3 \times 10^{12} \text{ cm}^{-2}$ in two locations inside electron and hole puddles. These points follow the logarithmic trend

$$\frac{v_F^*(n_e)}{10^6 \text{ m/s}} = \left(1.128 - 0.0799 \ln \frac{|n_e|}{10^{12} \text{ cm}^{-2}} \right). \quad (12)$$

We have taken in our calculations 34 combinations of $n = -8, -7, \dots, +7, +8$, and $B = 2, 5$ T to evaluate $v_F^*(n_e)$ in the same range.

TABLE II: Dielectric constants of surrounding medium ε , which provide the best least-square fittings of the experimental data from Ref. [16] at several selected v_F . The fittings are carried out in four screening models, described in Sec. II.

v_F , 10^6 m/s	Unscreened	Screened	Self-cons.	Self-cons.
	interaction $r_s = 0$	interaction $r_s = \frac{e^2}{\varepsilon \hbar v_F}$	screening $r_s = \frac{e^2}{\varepsilon \hbar (v_F^*)}$	screening $r_s = \frac{e^2}{\varepsilon \hbar v_F^*(n_e)}$
0.8	7.57	1.50	2.93	2.94
0.85	9.05	3.08	4.27	4.26
0.9	11.23	5.32	6.27	6.25
1	21.76	15.58	16.12	16.09

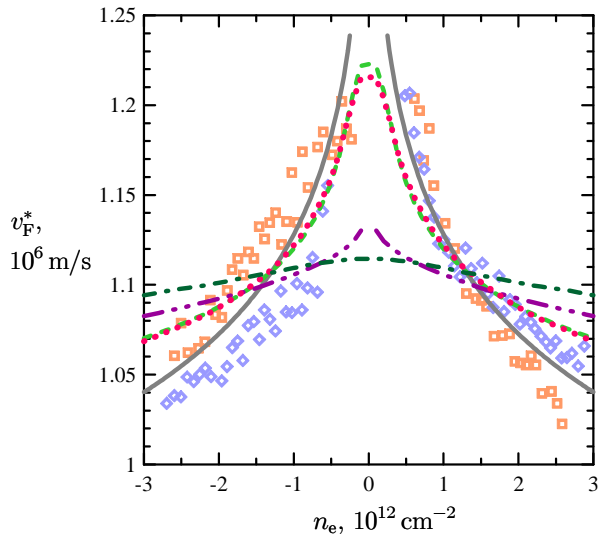


FIG. 6: The same as Fig. 4, but for experimental points of [16] with the logarithmic trend (12).

Similarly to the analysis of the previous experiment, we have carried out the least-square fitting by adjusting ε , and the results are given in Table II. In the 3rd model we take the average experimental Fermi velocity $\langle v_F^* \rangle = 1.105 \times 10^6$ m/s. Here we see the same regularities as in the previous analysis, but the optimal dielectric constants turn out to be larger, because here the measured renormalized Fermi velocities are generally lower than in [15] due to a stronger screening from the substrate. The best results with $v_F = 0.85 \times 10^6$ m/s in the self-consistent screening models provide $\varepsilon \approx 4-4.5$ which are close to the experimental $\varepsilon = 3.15$ [16] corresponding to graphene on the hexagonal boron nitride substrate. The best fits at $v_F = 0.85 \times 10^6$ m/s in the four screening models, corresponding to the entries in the second row of Table II, are shown in Fig. 5.

Again, we see that the unscreened interaction cannot provide a sufficiently rapid growth of v_F^* near the charge neutrality point. To illustrate the effect of the screening weakening at small carrier densities, we compare in Fig. 6 the calculations with the polarizability dependent on n_e and with that “frozen” at the filling factor $\nu = -14$. Similarly to Fig. 3, this effect turns out to be crucial to correctly reproduce the experimental data of [16].

V. CONCLUSIONS

Using the statically screened Coulomb interaction in the random-phase approximation, we carried out the many-body calculations of renormalized Landau level energies E_n^* in graphene in quantizing magnetic field. Fitting a set of E_n^* at different (n, B) by the formula (2), we evaluated the renormalized Fermi velocity v_F^* as a function of the carrier density n_e and compared our cal-

culations with the two scanning tunneling spectroscopy experiments [15, 16]. We achieved good agreement using the bare Fermi velocity $v_F = 0.85 \times 10^6$ m/s and the realistic values of the dielectric constant ε as the model parameters. The same value of v_F proved to be optimal in our previous work [32] where the cyclotron resonance and magneto-Raman scattering experimental data were described.

Our analysis allows us to draw the following main conclusions. First, the characterization of several renormalized energies E_n^* of different Landau levels n at different magnetic fields B at once with a single renormalized Fermi velocity v_F^* , assumed in many experimental works [9–16], generally works very well. However there exist small, but systematic deviations from the formula (2), both predicted by the theory and found in some experiments. In particular, the logarithmic decrease of v_F^* with increasing B was measured in magneto-Raman scattering [22, 23]. Small deviations from the linear fits (2), similar to those presented in Fig. 1 can be noted in the results of several other experimental works [12, 14, 45] and thus can possibly be attributed to many-body effects.

Second, the screening of Coulomb interaction is necessary to achieve a quantitative agreement between the theory and the experiments with realistic values of v_F and ε . Besides, the calculations without the screening fail to reproduce the rapid growth of v_F^* on approach to the charge neutrality point reported in [15, 16]. It can be reproduced only with taking into account that the screening becomes weaker when the carrier density decreases.

Third, the self-consistent weakening of the screening due to interaction-induced enlargement of virtual electron transition energies is also important to obtain quantitatively correct theoretical results. In our previous work [32], we made the same conclusion based on the analysis of the other experiments [17, 22]. In this work, we additionally demonstrate that the rapidly converging iterative self-consistent calculations of the Landau level energies and polarizability are possible in the case of graphene in a magnetic field.

Finally, we note that although the logarithmic growth of the quasiparticle velocity v_F^* , predicted when the particle momentum approaches the Dirac point $k \rightarrow 0$ in undoped graphene [1, 3, 4], is similar to the growth of v_F^* in doped graphene when the carrier density decreases $n_e \rightarrow 0$, their physical origins are not the same. In the second case, the key role of the carrier-density dependent screening should be taken into account.

Acknowledgments

The authors are grateful to Andrey D. Zabolotskiy for helpful discussions. The work of Y.E.L. was supported by the Program for Basic Research of the National Research University Higher School of Economics, and the work of A.A.S. was supported by the Foundation for the advancement of theoretical physics “BASIS”.

-
- [1] A. H. Castro Neto, F. Guinea, N. M. R. Peres, K. S. Novoselov, and A. K. Geim, The electronic properties of graphene, *Rev. Mod. Phys.* **81**, 109 (2009).
 - [2] D. N. Basov, M. M. Fogler, A. Lanzara, F. Wang, and Y. Zhang, Colloquium: Graphene spectroscopy, *Rev. Mod. Phys.* **86**, 959 (2014).
 - [3] V. N. Kotov, B. Uchoa, V. M. Pereira, F. Guinea, and A. H. Castro Neto, Electron-Electron Interactions in Graphene: Current Status and Perspectives, *Rev. Mod. Phys.* **84**, 1067 (2012).
 - [4] J. González, F. Guinea, and M. A. H. Vozmediano, Non-Fermi liquid behavior of electrons in the half-filled honeycomb lattice (A renormalization group approach), *Nucl. Phys. B* **424**, 595 (1994).
 - [5] M. O. Goerbig, Electronic properties of graphene in a strong magnetic field, *Rev. Mod. Phys.* **83**, 1193 (2011).
 - [6] M. Orlita and M. Potemski, Dirac electronic states in graphene systems: optical spectroscopy studies, *Semicond. Sci. Technol.* **25**, 063001 (2010).
 - [7] V. A. Miransky and I. A. Shovkovy, Quantum field theory in a magnetic field: From quantum chromodynamics to graphene and Dirac semimetals, *Phys. Rep.* **576**, 1 (2015).
 - [8] L.-J. Yin, K.-K. Bai, W. Wang, S.-Y. Li, Y. Zhang, and L. He, Landau quantization of Dirac fermions in graphene and its multilayers, *Front. Phys.* **12**, 127208 (2017).
 - [9] G. Li and E. Y. Andrei, Observation of Landau levels of Dirac fermions in graphite, *Nature Phys.* **3**, 623 (2007).
 - [10] G. Li, A. Luican, and E. Y. Andrei, Scanning Tunneling Spectroscopy of Graphene on Graphite, *Phys. Rev. Lett.* **102**, 176804 (2009).
 - [11] A. Luican, G. Li, and E. Y. Andrei, Scanning tunneling microscopy and spectroscopy of graphene layers on graphite, *Solid State Commun.* **109**, 1151 (2009).
 - [12] D. L. Miller, K. D. Kubista, G. M. Rutter, M. Ruan, W. A. de Heer, P. N. First, and J. A. Stroscio, Observing the Quantization of Zero Mass Carriers in Graphene, *Science* **324**, 924 (2009).
 - [13] Y. J. Song, A. F. Otte, Y. Kuk, Y. Hu, D. B. Torrance, P. N. First, W. A. de Heer, H. Min, S. Adam, M. D. Stiles, A. H. MacDonald, and J. A. Stroscio, High-resolution tunnelling spectroscopy of a graphene quartet, *Nature* **467**, 185 (2010).
 - [14] L.-J. Yin, S.-Y. Li, J.-B. Qiao, J.-C. Nie, and L. He, Landau quantization in graphene monolayer, Bernal bilayer, and Bernal trilayer on graphite surface, *Phys. Rev. B* **91**, 115405 (2015).
 - [15] A. Luican, G. Li, and E. Y. Andrei, Quantized Landau level spectrum and its density dependence in graphene, *Phys. Rev. B* **83**, 041405(R) (2011).
 - [16] J. Chae, S. Jung, A. F. Young, C. R. Dean, L. Wang, Y. Gao, K. Watanabe, T. Taniguchi, J. Hone, K. L. Shepard, P. Kim, N. B. Zhitenev, and J. A. Stroscio, Renormalization of the graphene dispersion velocity determined from

- scanning tunneling spectroscopy, *Phys. Rev. Lett.* **109**, 116802 (2012).
- [17] Z. Jiang, E. A. Henriksen, L. C. Tung, Y.-J. Wang, M. E. Schwartz, M. Y. Han, P. Kim, and H. L. Stormer, Infrared spectroscopy of Landau levels of graphene, *Phys. Rev. Lett.* **98**, 197403 (2007).
- [18] Z. Jiang, E. A. Henriksen, P. Cadden-Zimansky, L.-C. Tung, Y.-J. Wang, P. Kim, and H. L. Stormer, Cyclotron resonance near the charge neutrality point of graphene, *AIP Conf. Proc.* **1399**, 773 (2011).
- [19] E. A. Henriksen, P. Cadden-Zimansky, Z. Jiang, Z. Q. Li, L.-C. Tung, M. E. Schwartz, M. Takita, Y.-J. Wang, P. Kim, and H. L. Stormer, Interaction-induced shift of the cyclotron resonance of graphene using infrared spectroscopy, *Phys. Rev. Lett.* **104**, 067404 (2010).
- [20] B. J. Russell, B. Zhou, T. Taniguchi, K. Watanabe, and E. A. Henriksen, Many-particle effects in the cyclotron resonance of encapsulated monolayer graphene, arXiv:1709.00435.
- [21] S. Berciaud, M. Potemski, and C. Faugeras, Probing electronic excitations in mono- to pentalayer graphene by micro magneto-Raman spectroscopy, *Nano Lett.* **14**, 4548 (2014).
- [22] C. Faugeras, S. Berciaud, P. Leszczynski, Y. Henni, K. Nogajewski, M. Orlita, T. Taniguchi, K. Watanabe, C. Forsythe, P. Kim, R. Jalil, A. K. Geim, D. M. Basko, and M. Potemski, Landau level spectroscopy of electron-electron interactions in graphene, *Phys. Rev. Lett.* **114**, 126804 (2015).
- [23] C. Faugeras, M. Orlita, and M. Potemski, Raman scattering of graphene based systems in high magnetic fields, arXiv:1706.06303.
- [24] J. Sonntag, S. Reichardt, L. Wirtz, B. Beschoten, M. I. Katsnelson, F. Libisch, and C. Stampfer, Impact of Many-Body Effects on Landau Levels in Graphene, arXiv:1712.05648.
- [25] A. Iyengar, J. Wang, H. A. Fertig, and L. Brey, Excitations from filled Landau levels in graphene, *Phys. Rev. B* **75**, 125430 (2007).
- [26] Yu. A. Bychkov and G. Martinez, Magnetoplasmon excitations in graphene for filling factors $\nu \leq 6$, *Phys. Rev. B* **77**, 125417 (2008).
- [27] R. Roldán, J.-N. Fuchs, and M. O. Goerbig, Spin-flip excitations, spin waves, and magnetoexcitons in graphene Landau levels at integer filling factors, *Phys. Rev. B* **82**, 205418 (2010).
- [28] Y. Barlas, W.-C. Lee, K. Nomura, and A. H. MacDonald, Renormalized Landau levels and particle-hole symmetry in graphene, *Int. J. Mod. Phys. B* **23**, 2634 (2009).
- [29] K. Shizuya, Many-body corrections to cyclotron resonance in monolayer and bilayer graphene, *Phys. Rev. B* **81**, 075407 (2010).
- [30] K. Shizuya, Many-body corrections to cyclotron resonance in graphene, *J. Phys.: Conf. Ser.* **334**, 012046 (2011).
- [31] K. Shizuya, Direct-exchange duality of the Coulomb interaction and collective excitations in graphene in a magnetic field, *Int. J. Mod. Phys. B* **31**, 1750176 (2017).
- [32] A. A. Sokolik, A. D. Zabolotskiy, and Yu. E. Lozovik, Many-body effects of Coulomb interaction on Landau levels in graphene, *Phys. Rev. B* **95**, 125402 (2017).
- [33] L. A. Chizhova, J. Burgdorfer, and F. Libisch, Magneto-optical response of graphene: Probing substrate interactions, *Phys. Rev. B* **92**, 125411 (2015).
- [34] E. V. Gorbar, V. P. Gusynin, V. A. Miransky, and I. A. Shovkovy, Coulomb interaction and magnetic catalysis in the quantum Hall effect in graphene, *Phys. Scr.* **T146**, 014018 (2012).
- [35] I. A. Shovkovy and L. Xia, Generalized Landau level representation: Effect of static screening in the quantum Hall effect in graphene, *Phys. Rev. B* **93**, 035454 (2016).
- [36] X.-Z. Yan and C. S. Ting, Integer quantum Hall effect of interacting electrons in graphene, *Phys. Rev. B* **95**, 075107 (2017).
- [37] N. Menezes, V. S. Alves, and C. M. Smith, The influence of a weak magnetic field in the Renormalization-Group functions of (2+1)-dimensional Dirac systems, *Eur. Phys. J. B* **89**, 271 (2016).
- [38] G. Gumbs, A. Balassis, D. Dahal, and M. L. Glasser, Thermal smearing and screening in a strong magnetic field for Dirac materials in comparison with the two-dimensional electron liquid, *Eur. Phys. J. B* **89**, 234 (2016).
- [39] P. K. Pyatkovskiy and V. P. Gusynin, Dynamical polarization of graphene in a magnetic field, *Phys. Rev. B* **83**, 075422 (2011).
- [40] R. Roldán, J.-N. Fuchs, and M. O. Goerbig, Collective modes of doped graphene and a standard two-dimensional electron gas in a strong magnetic field: Linear magnetoplasmons versus magnetoexcitons, *Phys. Rev. B* **80**, 085408 (2009).
- [41] R. Roldán, M. O. Goerbig, and J.-N. Fuchs, The magnetic field particle-hole excitation spectrum in doped graphene and in a standard two-dimensional electron gas, *Semicond. Sci. Technol.* **25**, 034005 (2010).
- [42] M. Tahir and K. Sabeeh, Inter-band magnetoplasmons in mono- and bilayer graphene, *J. Phys.: Condens. Matter* **20**, 425202 (2008).
- [43] Yu. E. Lozovik, A. A. Sokolik, and A. D. Zabolotskiy, Quantum capacitance and compressibility of graphene: The role of Coulomb interactions, *Phys. Rev. B* **91**, 075416 (2015).
- [44] G. L. Yu, R. Jalil, B. Belle, A. S. Mayorov, P. Blake, F. Schedin, S. V. Morozov, L. A. Ponomarenko, F. Chiappini, S. Wiedmann, U. Zeitler, M. I. Katsnelson, A. K. Geim, K. S. Novoselov, and D. C. Elias, Interaction phenomena in graphene seen through quantum capacitance, *Proc. Natl. Acad. Sci. USA* **110**, 3282 (2013).
- [45] Z.-G. Chen, Z. Shi, W. Yang, X. Lu, Y. Lai, H. Yan, F. Wang, G. Zhang, and Z. Li, Observation of an intrinsic bandgap and Landau level renormalization in graphene/boron-nitride heterostructures, *Nature Commun.* **5**, 4461 (2014).